Characterization and Description of a Spectrum Unfolding Method for the CATRiNA neutron detector array

A. B. Morelock^a, J. F. Perello^a, S. Almaraz-Calderon^a, B. W. Asher^a, K. Brandenburg^b, J. Derkin^b, G. Hamad^b, Y. Jones-Alberty^b, E. Lopez Saavedra^a, T. Massey^b, Z. Meisel^b, N. Singh^b, D. Soltesz^b, S. K. Subedi^b, A. Voinov^b, J. Warren^b

^aDepartment of Physics, Florida State University, Tallahassee, Florida, USA ^bDepartment of Physics and Astronomy, Ohio University, Athens, Ohio, USA

Abstract

The CATRiNA deuterated neutron detector array at Florida State University consists of 16 2"× 2" and 16 4"× 2" EJ-315 detectors with characteristic light output and pulse-shape discrimination capabilities. The unique properties of the detectors, in part due to the anisotropic nature of (d,n) scattering, are used to extract the energy of neutrons via pulse-height spectrum unfolding. The unfolding method uses the light output and response matrix of the detectors to extract neutron energies, independent of the traditional time-of-flight (ToF) technique. Detailed response matrices of the CATRiNA detectors were measured at the Edwards Accelerator Laboratory at Ohio University via the ⁹Be(d,n) and ²⁷Al(d,n) reactions. Full characterization of the detectors using digital electronics, as well as a description of the unfolding method are reported.

1. Introduction

The efficient and accurate detection of neutrons is essential in basic nuclear science as well as nuclear

nonproliferation and safeguards applications [1]. However, the neutral-charge nature of the neutron makes

4 its detection challenging. Since neutrons carry no charge, they are indirectly studied through their interac-

5 tions with other nuclei. Some neutron detectors are based on thermal reactions, where neutrons interacting

6 with certain nuclei can cause a nuclear reaction. The products of these reactions, including gamma-rays,

protons, alpha-particles, and fission fragments, initiate the detection process. These types of detectors are

8 usually surrounded by a moderating material to maximize detection efficiency [2]. Other detectors rely on

the neutron scattering with a nucleus and transferring some of its kinetic energy to the recoiling nucleus.

 $\textit{Email addresses:} \texttt{abm17c@my.fsu.edu} \ (A.\ B.\ Morelock), \texttt{salmarazcalderon@fsu.edu} \ (S.\ Almaraz-Calderon) \ ($

If enough energy is transferred, the recoiling nucleus ionizes the material surrounding the point of interaction. This mechanism is only efficient for neutrons interacting with light nuclei, therefore, neutron detectors based on this principle often use hydrogen-based scintillating materials [2]. In such cases, the neutron's energy is typically determined via its time-of-flight (ToF), where a long flight path is needed to obtain good energy resolution. Consequently, the detectors must be placed a considerable distance from the reaction target, effectively decreasing the solid angle coverage of the detector array. An alternative method of extracting neutron energies without fully relying on ToF has been sought in order to efficiently optimize the solid angle coverage and size of the detector array.

The use of neutron detectors with deuterated scintillating material, rather than hydrogen-based scintil-18 lating material, has recently increased [3–6] due to unique features produced in the light output spectrum. Neutrons scattered with the deuterium in the scintillator will produce a characteristic forward recoil peak 20 and low valley in the light output spectrum [7]. This feature, due to the asymmetry of the cross section for 21 n-d scattering which peaks at backwards angles, extends across a large range of neutron energies. The char-22 acteristic light output spectra of deuterated scintillators can be used for the extraction of neutron energies using spectrum unfolding methods. The light output spectrum is analyzed using a statistical approach that 24 extracts the most probable neutron energy spectra using the detector's response matrix which is obtained 25 via the characterization of the detectors' response to a broad range of neutron energies. 26

The Compound Array for Transfer Reactions in Nuclear Astrophysics (CATRiNA) neutron detector array has been developed at Florida State University (FSU) [8]. This work discusses detector characterization, the measurement of response matrices, and the spectrum unfolding method used to obtain neutron energies with CATRiNA.

31 2. Detectors

27

28

29

30

The CATRiNA neutron detector array is composed of 32 deuterated-benzene (C_6D_6) liquid scintillators [9]. The CATRiNA detectors are currently of two sizes: 16 'small' detectors and 16 'large' detectors. The small detectors encapsulate the scintillating material in a 2" diameter \times 2" deep cylindrical aluminum cell and are coupled to Hamamatsu R7724 Photo-Multiplier Tubes (PMTs) [10]. The large detectors encapsulate the scintillating material in a 4" diameter \times 2" deep cylindrical aluminum cell which are coupled to ET Enterprise 9821B Photo-Multiplier Tubes (PMTs) [11]. Although the large detectors have been previously characterized [8], full characterization of the small detectors and further detailed characterization of the large detectors was needed in order to obtain detailed response matrices of both detector sizes under the

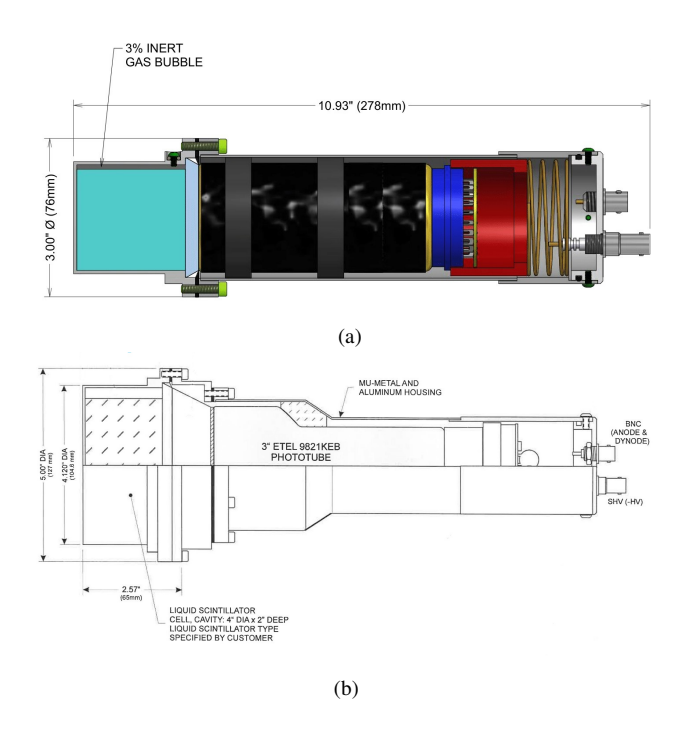


Figure 1: Schematic of the small neutron detector [9] with the scintillating material in a $2'' \times 2''$ Al cell in Figure 1a. Schematic of the large neutron detector [9] with the scintillating material in a $4'' \times 2''$ Al cell in Figure 1b.

Detector	Long	Short	Pre-Gate
4" by 2" EJ-315	196 ns	36 ns	100 ns
2" by 2" EJ-315	196 ns	24 ns	92 ns

Table 1: Optimized PSD timing gates applied to the small and large CATRiNA detectors.

same experimental conditions. Schematics of the small and large detectors are shown in Figures 1a and 1b. 40 The CATRINA detectors allow for the separation of neutron (n) and gamma-ray (γ) interactions using 41 their pulse shape discrimination (PSD) capabilities. By applying different integration timing gates to the 42 pulses collected from the detectors in the data acquisition system (DAQ), suitable n/γ separation can be achieved. In the present work three different timing gates were applied: Short, Long, and Pre-gate. These 44 gates were optimized for the different detectors, and the integration times are shown in Table 1. The Short 45 gate provides an integration for the rise time of the pulse and the Long gate provides an integration of the entire pulse. The Pre-gate sets the starting position of the Long and Short gates. A typical PSD plot is seen in Figure 2 where the PSD is plotted against the Long gate, or Pulse-Height. Here PSD is defined as the 48 difference between the Long gate and Short gate divided by the Long gate. From Fig. 2, it is observed that 49 neutron (inside the red contour) and gamma-ray events are well separated in two distinctive groups.

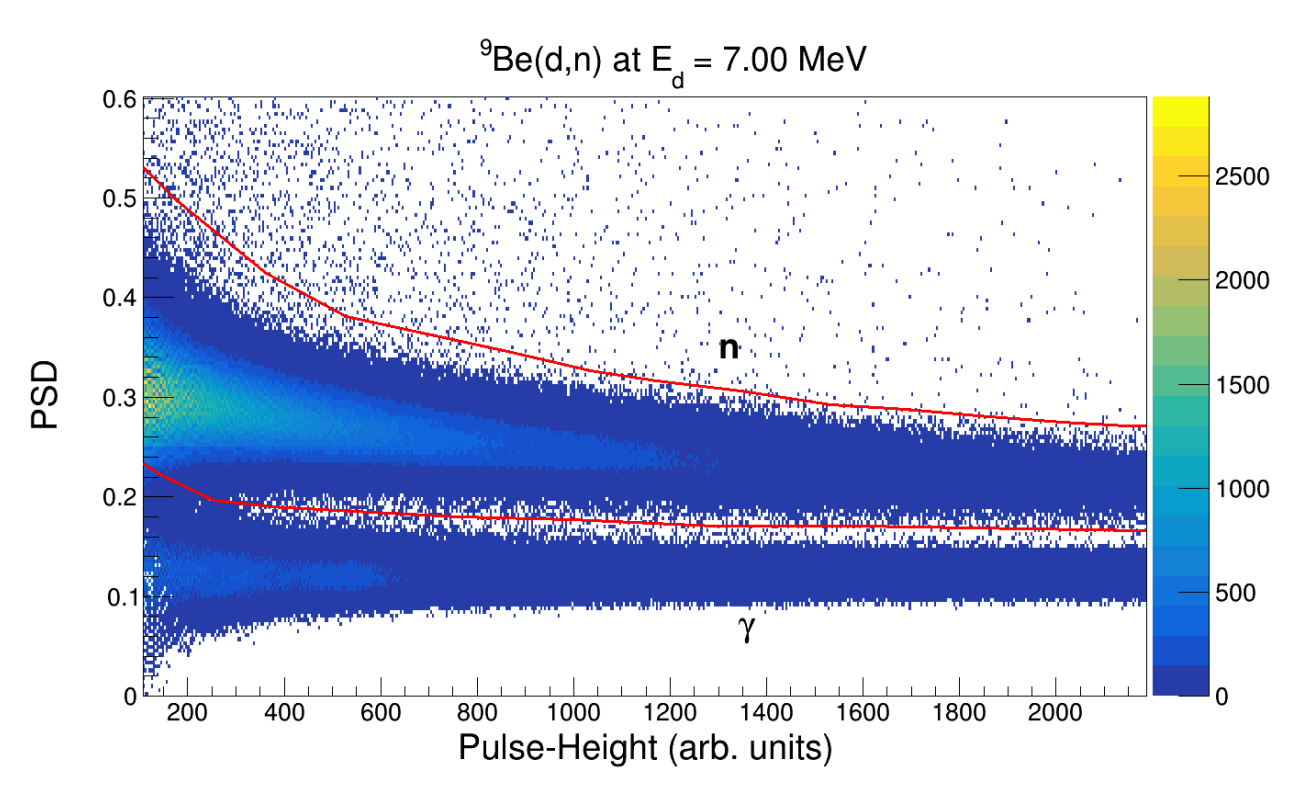


Figure 2: Typical Pulse-shape discrimination (PSD) plot obtained with one of the small $2'' \times 2''$ EJ-315 detector. The y-axis is defined as: PSD = (Long gate - Short gate)/ Long gate. The red contour encloses neutron events.

3. Measurement of the ⁹Be(d,n) and ²⁷Al(d,n) reactions

A measurement of the ⁹Be(d,n) and ²⁷Al(d,n) reactions using the CATRiNA detectors was performed at the Edwards Accelerator Laboratory at Ohio University [12]. The unique facility employees a beam swinger and neutron ToF tunnel for neutron measurements. For both reactions, a 4.5 MV tandem Van de Graff accelerator provided a pulsed deuterium beam with 1600 ns between beam pulses. Thick targets of ⁹Be and ²⁷Al were used as "white" neutron sources, producing a continuum of neutron energies dependent upon the energy of the deuterium beam [13–15].

The CATRiNA detectors (2 large and 2 small detectors) were placed at a flight path of 8.5 m inside the neutron ToF tunnel. The 9 Be(d,n) reaction occurred at $E_d = 7.00$ MeV with the beam swinger at 0° , while the 27 Al(d,n) reaction occurred at $E_d = 7.44$ MeV with the beam swinger at 120° [6, 13–15]. A background spectrum was obtained by using polyethylene bricks stacked at the entrance to the neutron ToF tunnel to block the face of the neutron detectors.

Calibration of the neutron detectors was determined using standard ¹³⁷Cs, ⁶⁰Co, and ²²Na gamma-ray 63 sources. A Compton edge is produced when maximum energy is transferred [7]. Since the location of the Compton edge is broadened due to the resolution of each of the detectors, it was placed at approximately 65 80% of the total peak height following the procedure outlined by Ref. [16]. The calibrated neutron detectors 66 adopt keVee (keV electron equivalent) units, defined as the particle energy required to generate 1 keVee of 67 light, which is 1 keV for an electron [2]. A set of two CAEN digitizers were used as data acquisition system 68 to acquire the neutron and timing signals, using CAEN's CoMPASS software. A CAEN V1730 14-bit 500 69 MS/s digitizer [17] acted as the "master" board while a CAEN V1725 14-bit 250 MS/s digitizer [18] was 70 the "slave" board. The signals from the anode of the PMT of the neutron detectors were sent to the V1725 71 digitizer. 72

A delayed beam pick-off timing pulse, modified using external NIM modules and the 'OR' output of the V1725 digitizer, was sent to the V1730 digitizer to make a ToF signal for each detector. Events were built offline using the timestamps of the signals.

4. Analysis and Characterization

76

Neutron events can be separated from gamma-ray events in the detectors using different integration times via the PSD method. Figure 3 shows ToF spectra for the ⁹Be(d,n) reaction. The red spectra displays the ToF of all events. The blue spectra displays only neutron events, which is accomplished by gating around

${}^{9}\text{Be}(d,n) \text{ at E}_{d} = 7.00 \text{ MeV}$ **Neutron Events** All Events 10⁴ 10³ 10² 10 0 100 200 300 400 500 600 700 800 ToF (ns)

Figure 3: ToF spectra from ${}^9\text{Be}(d,n)$ reaction for $2'' \times 2''$ EJ-315 neutron detector. All events are shown in red and neutron events gated from the PSD are shown in blue. The large peak close to 0 ns corresponds to the gamma flash associated with gamma-rays from the interaction of the beam with the target. This peak is strongly suppressed after applying the neutron gate.

- the neutron events as shown in Figure 2. An important characteristic of neutron detectors is to determine how low the n/γ threshold can be placed such that the neutron gate is clean from γ -ray events. For the small detectors a 55 keVee threshold was applied, while for the large detectors the threshold was placed at 85 keVee.
- Neutron energies are typically found using the non-relativistic ToF method:

$$E = \frac{1}{2}m\left(\frac{d}{t}\right)^2\tag{1}$$

where m is the mass of the neutron, d is the length of the flight path, and t is the neutron's time of flight [2]. In the present experiment quasi-monoenergetic neutron groups from the ${}^{9}\text{Be}(d,n)$ and the ${}^{27}\text{Al}(d,n)$ reactions where selected by applying tight cuts to their respective ToF spectra. The light output spectra of the neutrons associated with those ToF are extracted from the PSD plot. As an example, the light output spectra associated with neutron energies from $E_n = 1$ - 6 MeV in 1 MeV intervals from the ${}^{9}\text{Be}(d,n)$ reaction

${}^{9}\text{Be}(d,n)$ at $E_{d} = 7.00 \text{ MeV}$

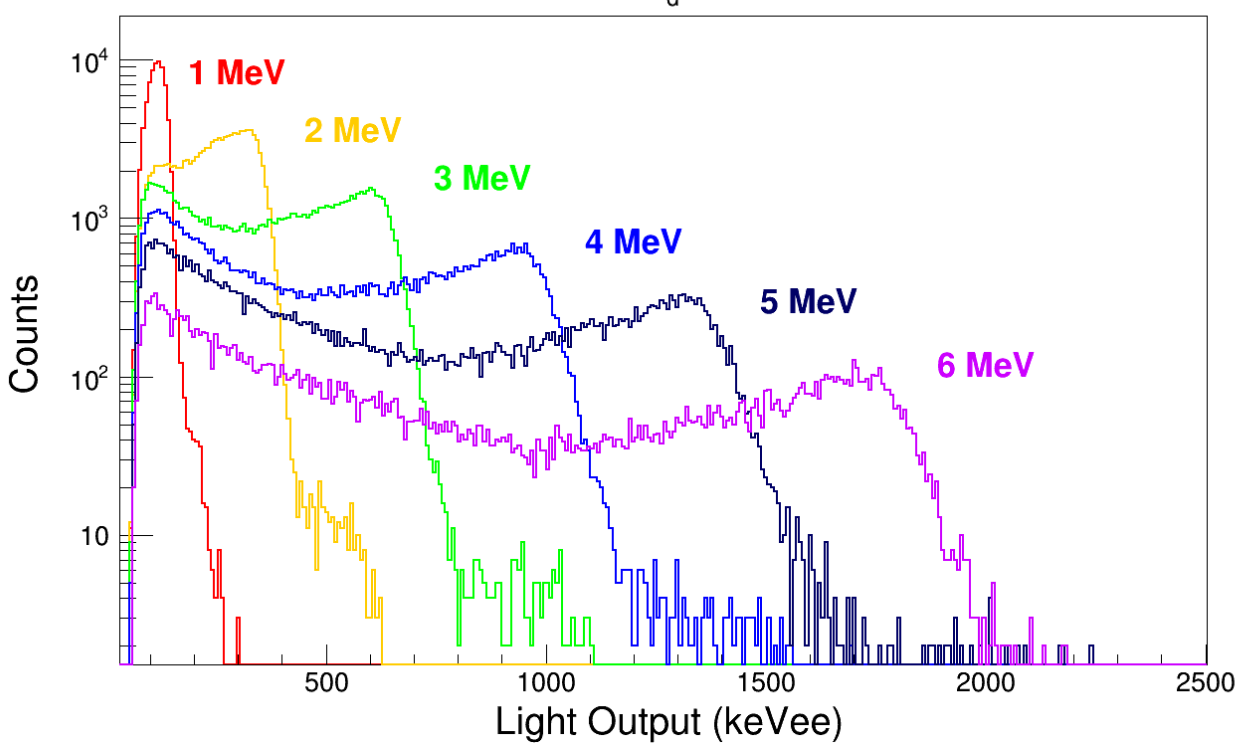


Figure 4: Light output spectra for several neutron energies extracted from $^9Be(d,n)$ reaction for a 2"× 2" EJ-315 neutron detector using PSD and ToF information.

are shown in Figure 4, where each color represents a different neutron energy. It can be observed that the characteristic recoil peak, or the shoulder at the end of the spectra, shifts farther to the right with increasing neutron energy as a consequence of the anisotropic d-n scattering.

The light output of the detector can then be parameterized as a function of the energy deposited by the neutron as described by equation:

$$L = aE_{dep} - b(1 - e^{-cE_{dep}})$$
 (2)

where the maximum deposited energy E_{dep} is taken at 8/9 of the neutron energy [5] and the light output L is taken at 80% of the recoil peak height to account for detector resolution [16]. The parameters a, b, and c in Eq. 2 for the small and large detectors are shown in Table 2. These values were obtained by fitting the data points in Figure 5, where the fit for the light output of the small detectors is shown in blue and the fit for the light output of the light output of the light output curves of the small and large detectors follow a similar trend.

A first order estimation of the resolution ΔL (FWHM) of the recoil peak can also be extracted from the

101

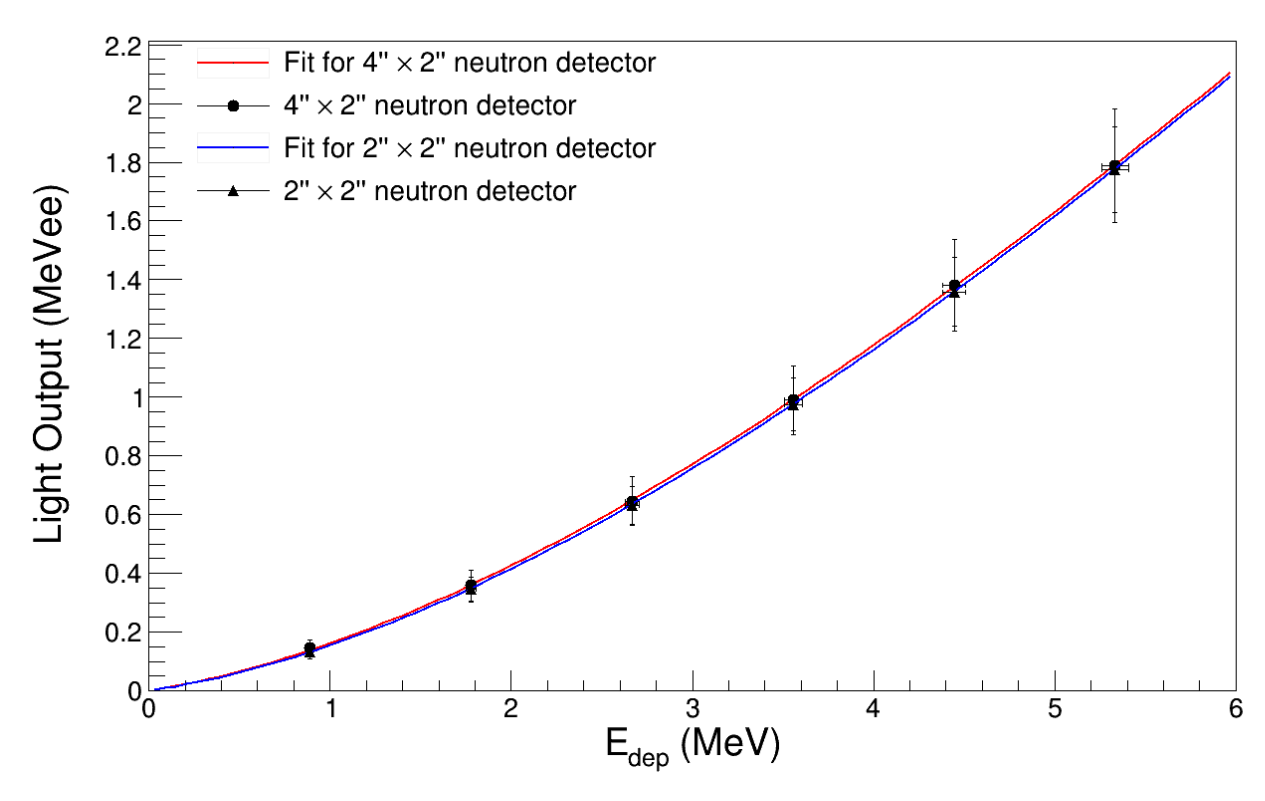


Figure 5: Measured light output for small and large detectors fit with Equation 2.

Detector	а	b	c
2"× 2" EJ-315	0.6193	2.036	0.2592
4"× 2" EJ-315	0.6109	1.946	0.2625

Table 2: Light output parameters a, b, and c for small and large detectors.

Detector	α	β	γ
2"× 2" EJ-315	0.0680	0.0615	0.0005
4"× 2" EJ-315	0.0956	0.0690	0.0005

Table 3: Resolution parameters α , β , and γ for small and large detectors.

quasi-monoenergetic light output spectra via Equation 3 [4].

110

111

112

115

116

117

119

120

$$\Delta L/L \simeq \frac{(L_{12.5} - L_{87.5})}{L_{50}} \tag{3}$$

In Equation 3 the parameters L_x are the light output values taken at the x^{th} percentage of the maximum recoil peak height. From these estimated resolution values, a more accurate function of the resolution can be extracted and described as a function of the light output taken at 80% of the recoil peak height. This function is defined in Equation 4 [16, 19].

$$\Delta L/L = \sqrt{\alpha^2 + \frac{\beta^2}{L} + \frac{\gamma^2}{L^2}} \tag{4}$$

In Equation 4 the parameter α is the locus dependent light transmission from the scintillating material to the photocathode, the parameter β describes the statistical behavior of the light production in the detector, and the parameter γ encompasses all noise contributions from the experimental setup [16].

The parameters α , β , and γ for the small and large CATRiNA detectors are shown in Table 3 and displayed in Figure 6 where the fit of the resolution for the small detectors is shown in blue and the fit for the large detectors is shown in red. It can be seen that at small light output (and neutron energy) values the resolution of the large and small detectors converge. However, for increasing light output the resolution values of the smaller detectors decreases by approximately 3% as compared to the larger detectors. This implies that the smaller detectors have improved resolution at larger neutron energies relative to their large counterparts.

The intrinsic efficiency of the CATRiNA neutron detectors was obtained using the ⁹Be(d,n) and ²⁷Al(d,n) reactions. Previous experiments [13–15] report neutron yields as a function of neutron energy and incident deuterium beam energy for these reactions. Using this data, the intrinsic efficiency of the large and small detectors were extracted for a variety of neutron energies. Figure 7 displays the intrinsic efficiency curves. The small detectors have a higher intrinsic efficiency than the large detectors due to the threshold dependency of the efficiency. For a lower threshold, the intrinsic efficiency increases.

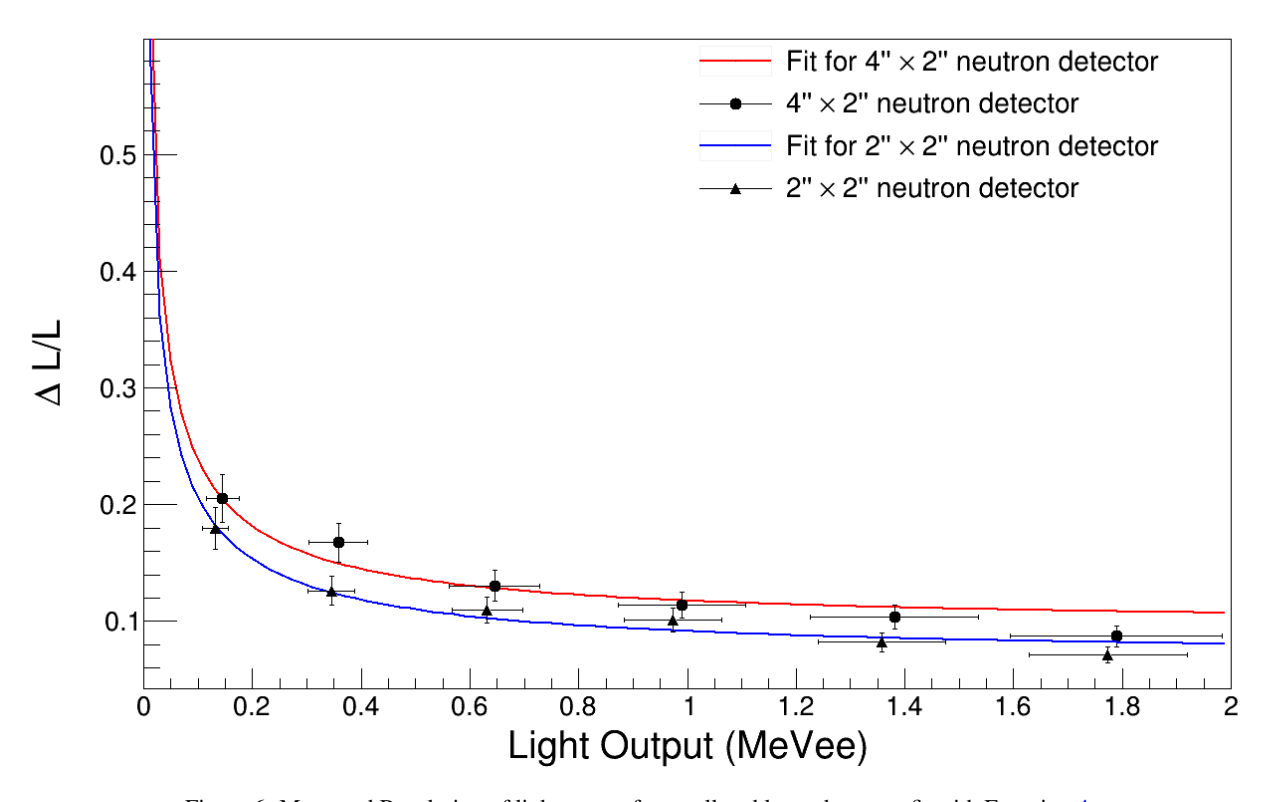


Figure 6: Measured Resolution of light output for small and large detectors fit with Equation 4.

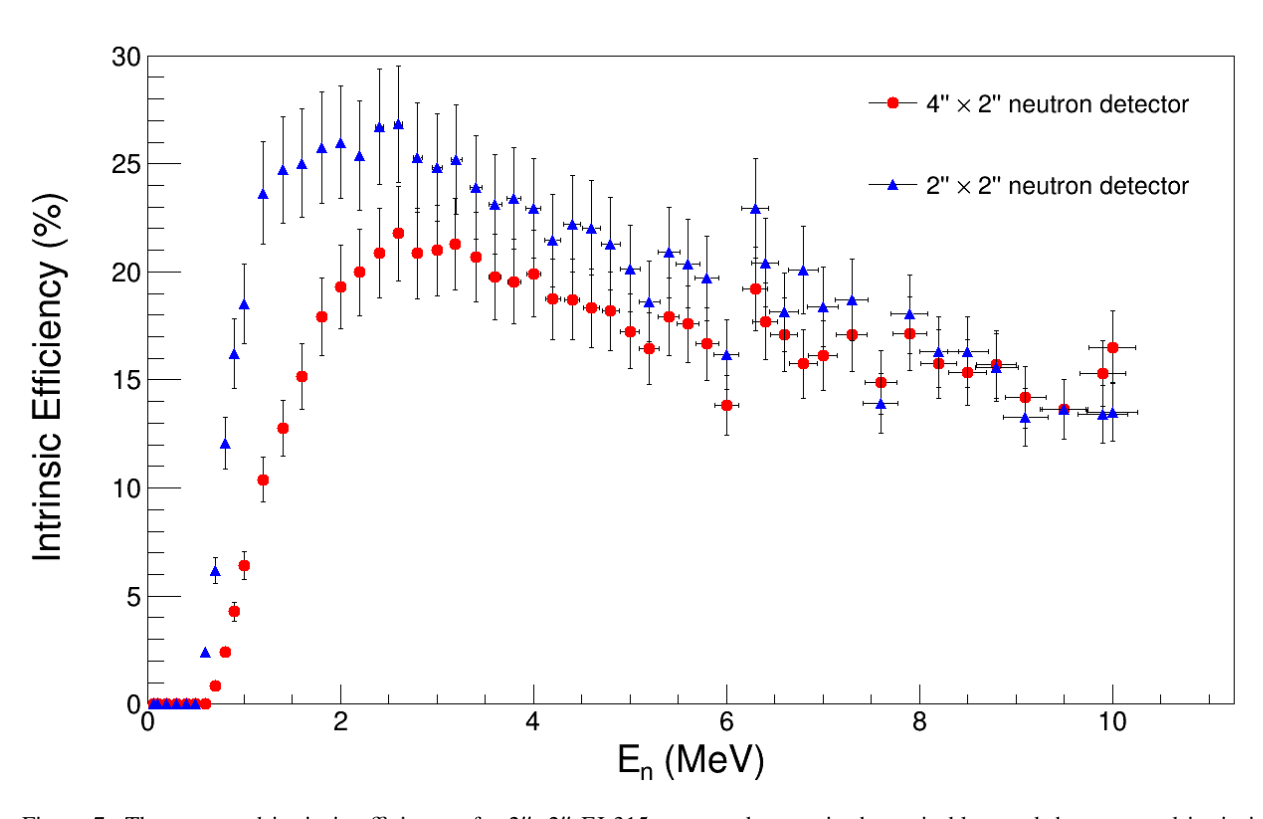


Figure 7: The measured intrinsic efficiency of a $2''\times2''$ EJ-315 neutron detector is shown in blue, and the measured intrinsic efficiency of a $4''\times2''$ EJ-315 neutron detector is shown in red.

For Figures 5 and 7 the error in the energy value is found by:

$$\Delta E/E = \sqrt{\left(\frac{2\Delta d}{d}\right)^2 + \left(\frac{2\Delta t}{t}\right)^2} \tag{5}$$

where Δd is largely from the width of the detector, d is the distance to the detector from the reaction target, Δt is the timing resolution, and t is the time it takes the neutron to travel distance d [2]. Energy resolution improves by increasing the distance, and therefore time t, between the reaction target and the detector. However, when placing detectors far away from the reaction target, the geometric efficiency decreases and there is a physical limit to how far away the detectors can be placed within a laboratory. To circumvent this, a method to extract neutron energies without relying on ToF known as spectrum unfolding was developed and it is discussed in the following section.

The response matrices of the CATRiNA detectors were created using neutrons from the ⁹Be(d,n) and ²⁷Al(d,n) reactions with an energy range of approximately 0.5 MeV to 9.54 MeV, binned in 40 keV increments. This range was chosen to ensure a sufficient amount of statistics in the response matrix. Higher neutron energies were present, however the intrinsic efficiency of the detectors steadily decreases for neutrons of larger energies. A consequence of this effect was observed in the response matrix for the 2"× 2" neutron detector, which also has low solid angle coverage. In Figure 8 at approximately 7.0 MeV the statistics for the higher energies decreases to a point where the recoil peak is no longer identifiable.

5. Spectrum Unfolding

123

131

132

133

136

137

138

Extraction of neutron energies from the light output spectra of liquid organic scintillators is a particularly challenging ill-posed problem that has been recently addressed using statistical unfolding algorithms [5, 6].

These unfolding algorithms aim to recover the energy spectrum that is most likely to have produced the measured response. A Bayesian method [20, 21] is used here to extract the neutron energies from the light output spectrum of the CATRiNA detectors.

The light output spectrum $\phi(L)$ extracted from a CATRiNA detector is described by a convolution of the detector's response function, denoted R(L, E) and the incident neutron energy spectrum $\psi(E)$:

$$\phi_i = \sum_{i=1}^{J} R_{ij} \psi_j, \quad i = 1, 2, ..., I$$
 (6)

where ϕ_i is the recorded count in the *i*-th light output bin, ψ_j is the neutron energy spectra, and R_{ij} is the response matrix [2]. Using Bayesian statistics[20, 21], the neutron energy spectrum $\psi(E)$ is then defined as a function of the response matrix and the light output spectrum according to the expression:

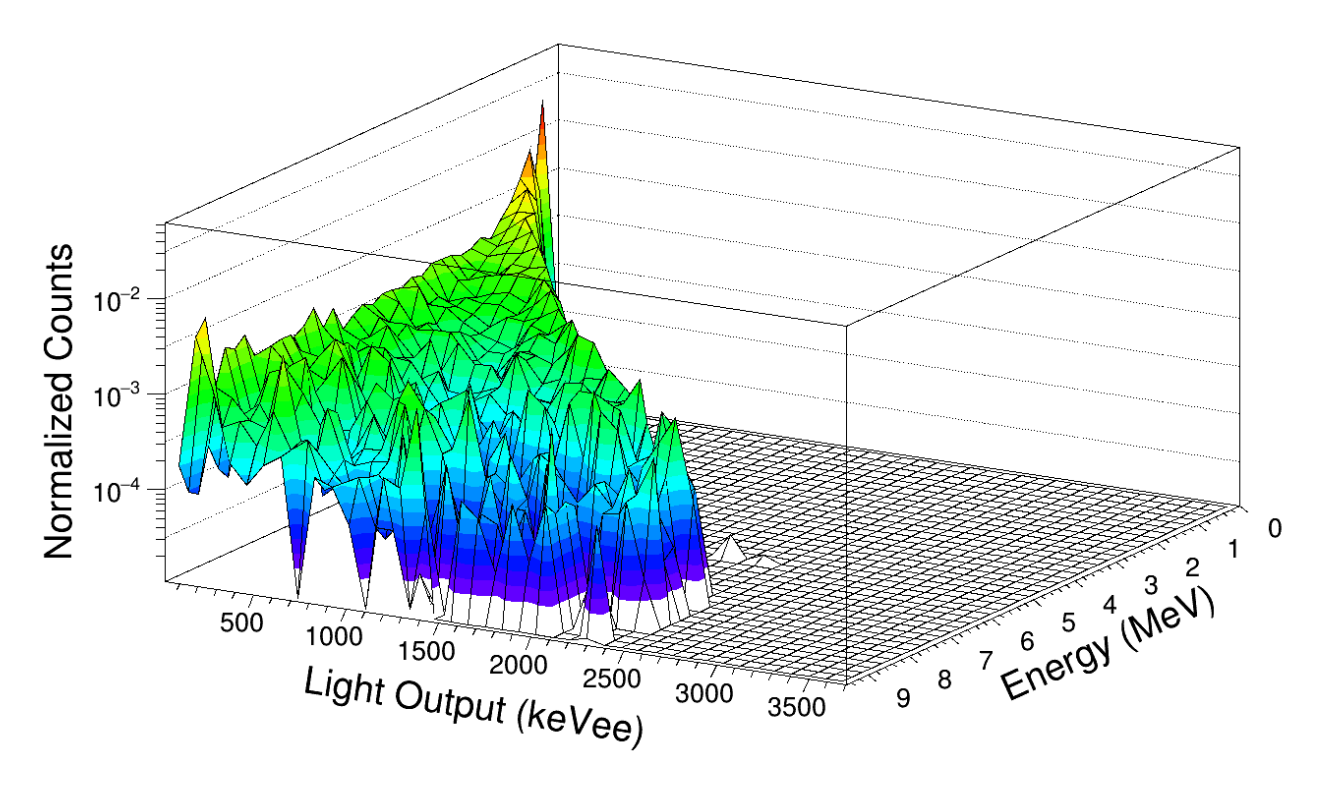


Figure 8: Measured response matrix of a 2"×2" EJ-315 neutron detector.

$$\psi_j^{k+1} = \psi_j^k \sum_{i=1}^I \frac{R_{ij}\phi_i}{\sum_{l=1}^J R_{il}\psi_l^k}, \quad j = 1, 2, ..., J$$
 (7)

where k is the number of estimates, or iterations. An unfolding algorithm that uses a statistical approach to solve Equation 7 has been developed. Up to a limit, each iteration will provide a new, better estimate of the neutron energy spectrum.

152 5.1. ANUBIS

A Novel Unfolding algorithm Using Bayesian Iterative Statistics (ANUBIS) is an unfolding algorithm developed for extracting neutron energies from the light output spectrum of the CATRiNA detectors. ANUBIS requires a detailed knowledge on the response matrix R_{ij} of the detector, calibration information, and the light output spectra $\phi(L)$ that is to be unfolded as inputs. The light output spectra $\phi(L)$ must match the binning of the response matrix. A threshold corresponding to the threshold of $\phi(L)$ is applied to the matrix before unfolding the input spectra. The response matrix R_{ij} must be normalized. Normalization is accomplished by summing the counts for each light output within each energy and setting them to unity. At each iteration, the program estimates an updated neutron energy spectra. Ideally, as the number of iterations

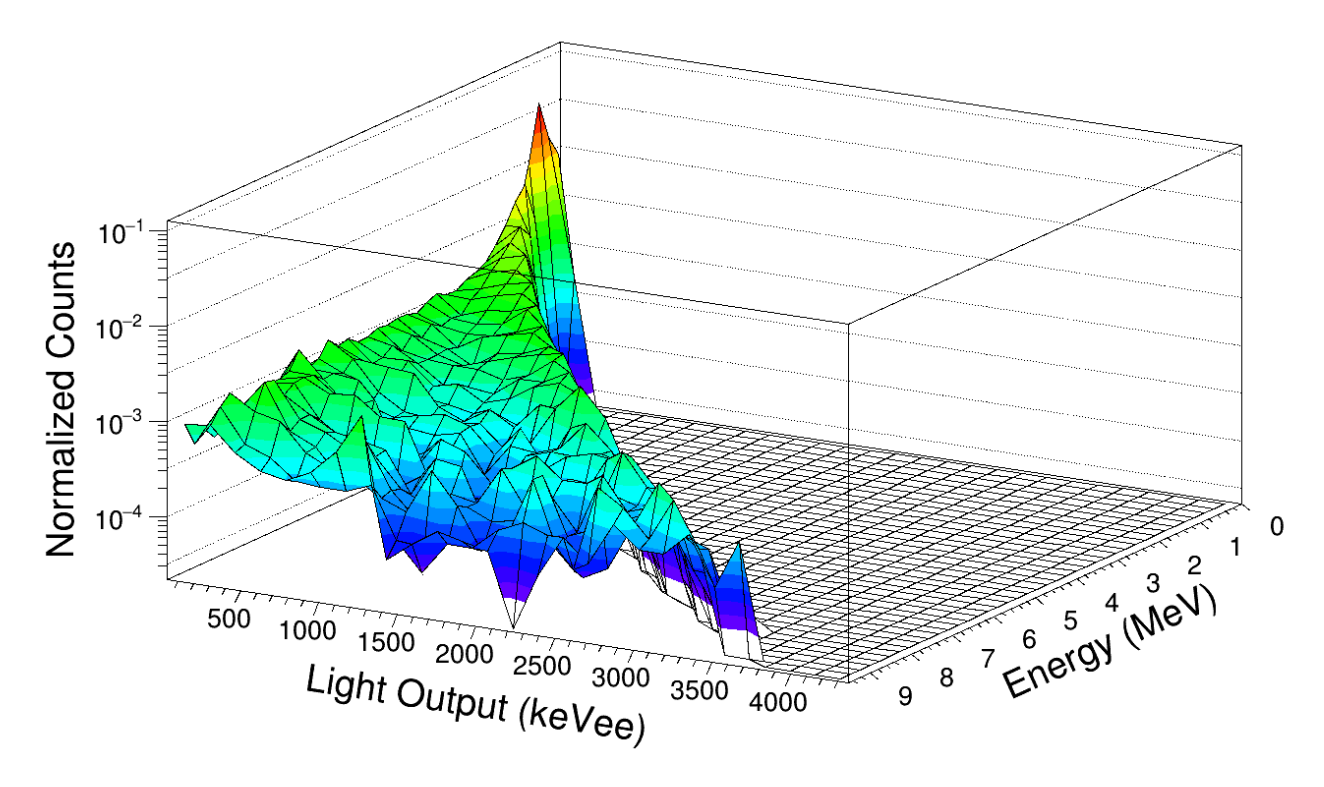


Figure 9: Measured response matrix of a 4"× 2" EJ-315 neutron detector.

grow, the unfolding algorithm should provide a new, improved estimate of the neutron energy spectra, i.e. as iterations increase the resolution of the energy peak improves.

As a self-consistency check, the light output spectra of quasi-monoenergetic neutron groups from the 9 Be(d,n) reaction were unfolded with ANUBIS. The light output spectra of these neutron energies can be seen in Figure 4. The unfolded neutron energy spectra is shown in Figure 10 for the $2'' \times 2''$ detector. Each energy peak corresponds to the light output curve of the same color. A similar check was performed for the $4'' \times 2''$ detector with similar results.

A stopping criteria using a chi-squared per degree of freedom (χ^2/DOF) has been implemented to find the "optimal" number of iterations. The chi-squared per degree of freedom is found by comparing the original light output spectra $\phi(L)$ and a refolded light output spectra $\phi'(L)$, and is defined as:

$$\chi^2/DOF = \frac{1}{I} \sum_{i=1}^{\infty} \frac{(\phi_i - \phi_i')^2}{\phi_i + \phi_i'}$$
 (8)

In Equation 8 the variable I is number of degrees of freedom, found such that it matches the binning of light output spectra. The refolded spectra ϕ'_i is made using the response matrix and the last estimate of the

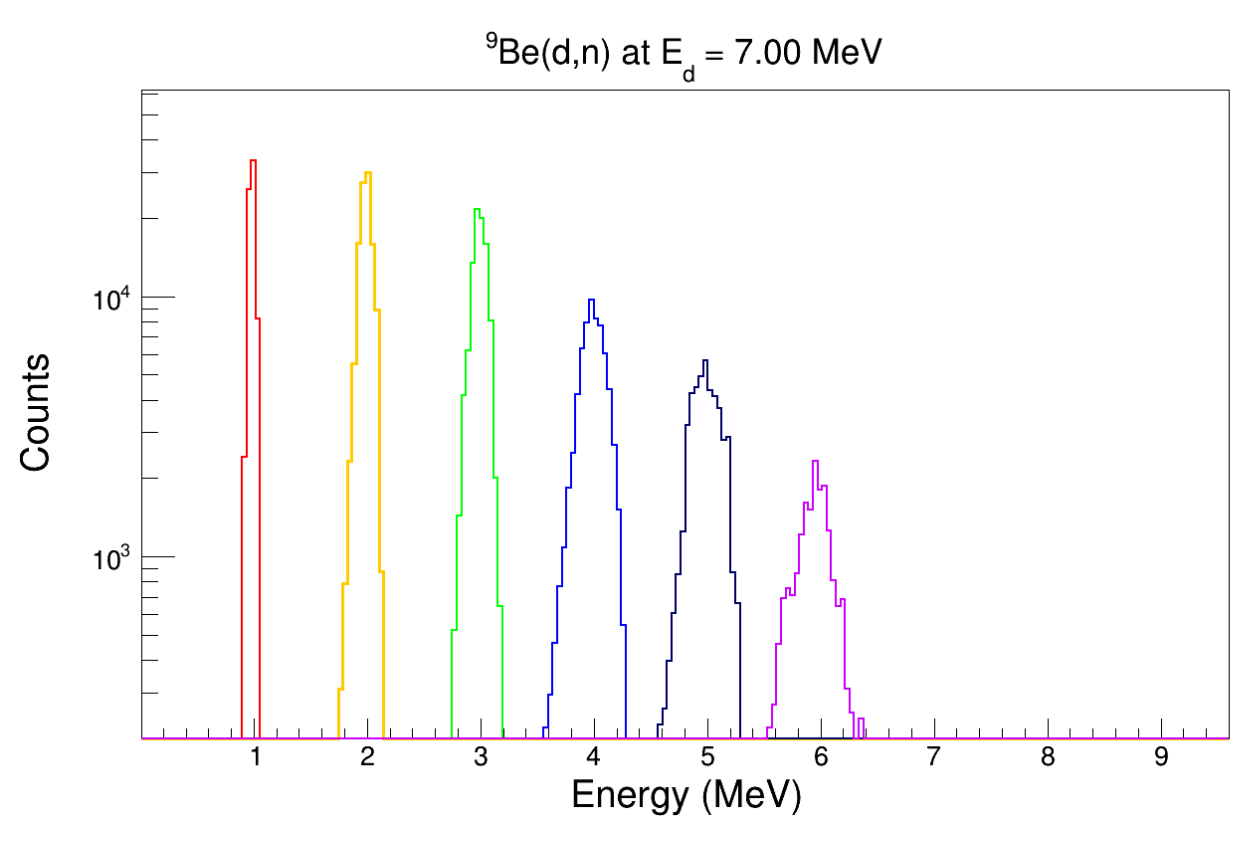


Figure 10: Unfolded neutron energy spectra from the $^9Be(d,n)$ reaction for the $2''\times 2''$ detector. The corresponding light output spectra for each energy can be found in Figure 4.

neutron energy spectra following Equation 6. Ideally, the value obtained in Equation 8 should converge to unity, but this does not always occur in practice due to fluctuating solutions [21]. To circumvent this a percent difference is found between the previous iteration's χ^2 and the current iteration's χ^2 . The program will continue to run until the percent difference is under a user defined value. As a fail safe to prevent the program running indefinitely, a maximum number of iterations is also set.

It was found that ANUBIS works best with a few hundred iterations at neutron energies where there are high statistics in both the response matrix and the light output spectra that is being unfolded. From our analysis, it is observed that if the number of iterations in the unfolding algorithm are too high (typically more than a thousand iterations), the refolded light output spectra develops small oscillations around the original light output spectra ϕ_i , but the unfolded energy spectra looses most definition and the peaks no longer approximate a Gaussian. This is an indication that ANUBIS is no longer realistically estimating the neutron energy spectra. The fluctuations are due to the fact that each bin of the light output spectra, or each discrete ϕ_i , acts as an independent degree of freedom and after a large amount of iterations the statistical fluctuations are amplified [21]. On the other end, it was also observed that if the program iterations are too few (typically less than 100 iterations), the original light output spectra ϕ_i is not accurately reproduced with the refolded light output spectra and the peak (or peaks) in the unfolded energy spectra has poor resolution.

Figure 11 shows how the percent difference for the unfolded neutron energy spectra of Figure 10 changes as a function of the amount of iterations performed. As the iterations increase, the percent difference between the previous iteration's χ^2 and the current iteration's χ^2 decreases until a point is reached where the value plateaus indicating the refolded light output spectra is now oscillating around the original light output spectra. To avoid too many iterations the percent difference was set to be less than 0.01%.

To prevent any ambiguity in stopping criteria as the χ^2/DOF approaches unity, the cases when $\chi^2/DOF \le 1$ and when $\chi^2/DOF \le 0.01\%$ were compared. Figure 12 displays the unfolded neutron energy spectra for a 4 MeV neutron from the ${}^9\text{Be}(\text{d,n})$ reaction using both stopping criteria. The red line is the estimation using a percent difference less than 0.01% which was achieved at 91 iterations and the blue line is the estimation when χ^2/DOF converges to unity which was achieved at 33 iterations. As shown in the figure, the estimation using the percent difference less than 0.01% stopping criteria has an improved resolution over the estimation from the convergent χ^2/DOF stopping criteria. These results were consistent along the several neutron energies analyzed in this work. By these results, it was determined that the stopping criteria that best models the data was the percent difference less than 0.01%.

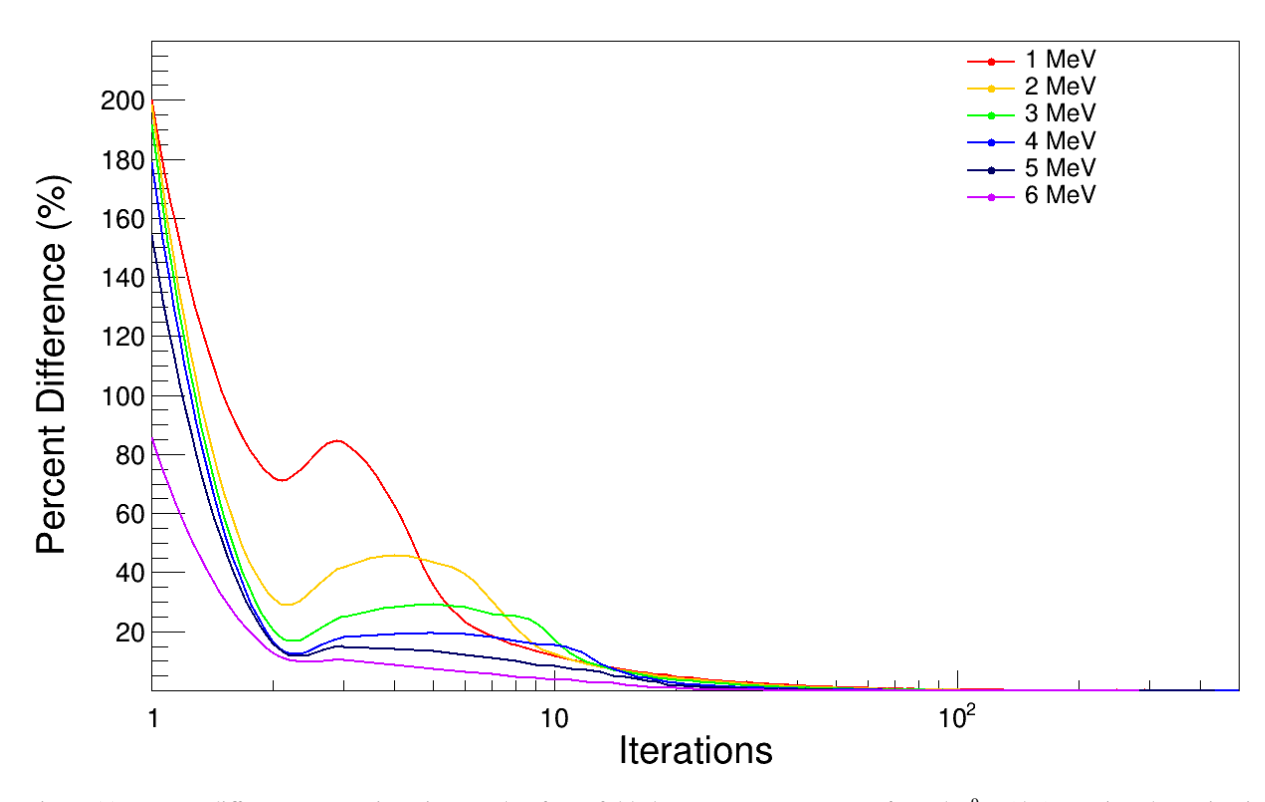


Figure 11: Percent difference versus iteration number for unfolded neutron energy spectra from the ⁹Be(d,n) reaction shown in Fig. 10. It was found that ANUBIS works best with a few hundred iterations at neutron energies where there are high statistics in both the response matrix and the light output spectra that is being unfolded.

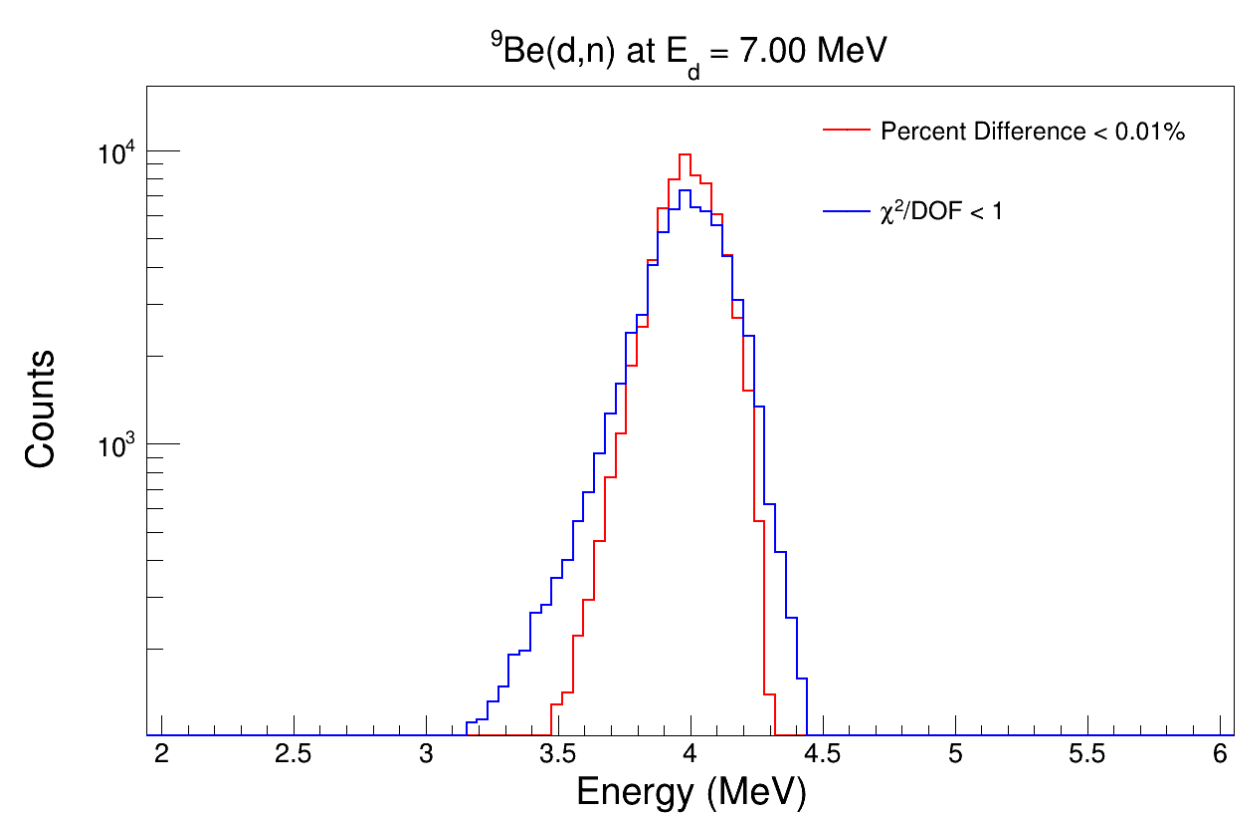


Figure 12: Unfolded neutron energy spectra for 4 MeV neutrons from the 9 Be(d,n) reaction. The "optimal" iteration (91 iterations) for the red peak is found by letting the percent difference from the χ^2/DOF be less than 0.01%. The "optimal" iteration (33 iterations) for the blue peak is found by letting the χ^2/DOF be less than unity.

6. Summary and Outlook

The CATRiNA neutron detector array now consists of 16 2"× 2" and 16 4"× 2" deuterated EJ-315 204 neutron detectors. Characterization of the array was preformed at the Edwards Accelerator Laboratory at 205 Ohio University via the ⁹Be(d,n) and ²⁷Al(d,n) reactions which provided a large range of neutron energies. 206 Analysis of the data provided valuable information on the characterization of the CATRiNA detectors, such 207 as the light output as a function of energy deposited, the resolution of the light output spectra as a function 208 of light output, as well as the intrinsic efficiency of the detectors. Detailed response matrices were also 209 extracted using results from the ⁹Be(d,n) and ²⁷Al(d,n) reactions. The ANUBIS code was developed to 210 perform spectrum unfolding of the light output spectra based on Bayesian statistics. ANUBIS uses the experimentally obtained response matrices of the CATRINA detectors to extract neutron energies. Analysis 212 of the unfolded and refolded spectra was performed to determine stopping criteria for the program. These 213 developments will be used in further experimental work to analyze neutron energies from various reactions 214 without fully relying on ToF information. 215

216 Acknowledgements

This work was supported by the National Science Foundation under Grants No. PHY-1712953 and No. PHY-2012522, the U.S. Department of Energy under Grants No. DE-FG02-88ER40387, No. DE-NA0003883, No. DE-NA0003909, and No. DE-SC0019042, and by the Stewardship Science Academic Alliance (USA) through the CENTAUR Center of Excellence under grant No. DE-NA0003841. The authors would like to thank Donald Carter and Gregory Leblanc from Ohio University for their help in completing the experimental setup.

References

223

224

225

226

227

228

237

- [1] S. A. Pozzi, T. H. Shin, M. Hua, W. Steinberger, M. M. Bourne, S. D. Clarke, Recent advances in neutron detection with organic scintillators, in: R. B. James, A. Burger, S. A. Payne (Eds.), Hard X-Ray, Gamma-Ray, and Neutron Detector Physics XXI, Vol. 11114, International Society for Optics and Photonics, SPIE, 2019, pp. 25 32. doi:10.1117/12.2530292. URL https://doi.org/10.1117/12.2530292
 - [2] G. F. Knoll, Radiation detection and measurement; 4th ed., Wiley, New York, NY, 2010.
- [3] P. E. Garrett, Descant the deuterated scintillator array for neutron tagging, Hyperfine Interactions 225 (1) (2014) 137–141.
 doi:10.1007/s10751-013-0891-9.
 URL https://doi.org/10.1007/s10751-013-0891-9
- [4] V. Bildstein, P. Garrett, J. Wong, D. Bandyopadhyay, J. Bangay, L. Bianco, B. Hadinia, K. Leach, C. Sumithrarachchi,
 S. Ashley, B. Crider, M. McEllistrem, E. Peters, F. Prados-Estévez, S. Yates, J. Vanhoy, Comparison of deuterated and normal liquid scintillators for fast-neutron detection, Nuclear Instruments and Methods in Physics Research Section A: Accelerators,
 Spectrometers, Detectors and Associated Equipment 729 (2013) 188 197. doi:https://doi.org/10.1016/j.nima.
 2013.06.082.
 - URL http://www.sciencedirect.com/science/article/pii/S0168900213009285

- [5] C. Lawrence, A. Enqvist, M. Flaska, S. Pozzi, F. Becchetti, Comparison of spectrum-unfolding performance of (ej315) and (ej309) liquid scintillators on measured 252cf pulse-height spectra, Nuclear Instruments and Methods in Physics Research, Section A: Accelerators, Spectrometers, Detectors and Associated Equipment 729 (2013) 924–929. doi:10.1016/j.nima. 2013.06.108.
- [6] M. Febbraro, B. Becker, R. deBoer, K. Brandenburg, C. Brune, K. Chipps, T. Danley, A. D. Fulvio, Y. Jones-Alberty, K. Macon, Z. Meisel, T. Massey, R. Newby, S. Pain, S. Paneru, S. Shahina, M. Smith, D. Soltesz, S. Subedi, I. Sultana, R. Toomey, Performance of neutron spectrum unfolding using deuterated liquid scintillator, Nuclear Instruments and Methods in Physics Research Section A: Accelerators, Spectrometers, Detectors and Associated Equipment 989 (2021) 164824. doi: https://doi.org/10.1016/j.nima.2020.164824.
 - URL https://www.sciencedirect.com/science/article/pii/S0168900220312213

248

249

250

285

290

- [7] F. Brooks, Development of organic scintillators, Nuclear Instruments and Methods 162 (1) (1979) 477 505. doi:https://doi.org/10.1016/0029-554X(79)90729-8.

 URL http://www.sciencedirect.com/science/article/pii/0029554X79907298
- [8] J. Perello, S. Almaraz-Calderon, B. Asher, L. Baby, N. Gerken, K. Hanselman, Characterization of the catrina neutron detector system, Nuclear Instruments and Methods in Physics Research Section A: Accelerators, Spectrometers, Detectors and Associated Equipment 930 (2019) 196 202. doi:https://doi.org/10.1016/j.nima.2019.03.084.
 URL http://www.sciencedirect.com/science/article/pii/S0168900219304267
- 255 [9] E. Technology, Deuterated ej315, https://eljentechnology.com/products/liquid-scintillators/ej-315 (Ac-256 cessed: 2018-04-15).
- 257 [10] Hamamatsu, R7724, https://www.hamamatsu.com/us/en/product/optical-sensors/pmt/pmt_tube-alone/ 258 head-on-type/R7724.html (Accessed: 2022-02-09).
- 259 [11] E. Enterprises, 9821b series, https://et-enterprises.com/products/photomultipliers/product/ 260 p9821b-series (Accessed: 2022-02-09).
- [12] Z. Meisel, G. Merz, S. Medvid, Influence of nuclear reaction rate uncertainties on neutron star properties extracted from x-ray burst model—observation comparisons, The Astrophysical Journal 872 (1) (2019) 84. doi:10.3847/1538-4357/aafede.
 URL http://dx.doi.org/10.3847/1538-4357/aafede
- 264 [13] J. W. Meadows, The 9be(d, n) thick-target neutron spectra for deuteron energies between 2.6 and 7.0 mev, Nuclear Instruments and Methods in Physics Research Section A: Accelerators, Spectrometers, Detectors and Associated Equipment 324 (1) (1993) 239-246. doi:https://doi.org/10.1016/0168-9002(93)90983-0.

 URL https://www.sciencedirect.com/science/article/pii/0168900293909830
- T. N. Massey, S. Al-Quraishi, C. E. Brient, J. F. Guillemette, S. M. Grimes, D. Jacobs, J. E. O'Donnell, J. Oldendick,
 R. Wheeler, A measurement of the 27al (d, n) spectrum for use in neutron detector calibration, Nuclear Science and Engineering 129 (2) (1998) 175–179. arXiv:https://doi.org/10.13182/NSE98-A1971, doi:10.13182/NSE98-A1971.
 URL https://doi.org/10.13182/NSE98-A1971
- 272 [15] T. N. Massey, D. K. Jacobs, S. I. Al-Quraishi, S. M. Grimes, C. E. Brient, W. B. Howard, J. C. Yanch, Study of the be(p,n)
 273 and be(d,n) source reactions, Journal of Nuclear Science and Technology 39 (sup2) (2002) 677–680. arXiv:https://doi.
 274 org/10.1080/00223131.2002.10875190, doi:10.1080/00223131.2002.10875190.
 275 URL https://doi.org/10.1080/00223131.2002.10875190
- [16] G. Dietze, H. Klein, Gamma-calibration of ne 213 scintillation counters, Nuclear Instruments and Methods in Physics Research 193 (3) (1982) 549-556. doi:https://doi.org/10.1016/0029-554X(82)90249-X.
 URL https://www.sciencedirect.com/science/article/pii/0029554X8290249X
- 279 [17] Caen, V1730/v1730s, https://www.caen.it/products/v1730/ (Accessed: 2018-04-15).
- 280 [18] Caen, V1725/v1725s, https://www.caen.it/products/v1725/ (Accessed: 2022-02-09).
- [19] C. C. Lawrence, A. Enqvist, M. Flaska, S. A. Pozzi, A. Howard, J. Kolata, F. Becchetti, Response characterization for an ej315 deuterated organic-liquid scintillation detector for neutron spectroscopy, Nuclear Instruments and Methods in Physics Research Section A: Accelerators, Spectrometers, Detectors and Associated Equipment 727 (2013) 21 28. doi:https://doi.org/10.1016/j.nima.2013.05.172.
 - URL http://www.sciencedirect.com/science/article/pii/S0168900213007948
- 286 [20] L. B. Lucy, An iterative technique for the rectification of observed distributions, 79 (1974) 745. doi:10.1086/111605.
- [21] G. D'Agostini, A multidimensional unfolding method based on bayes' theorem, Nuclear Instruments and Methods in Physics
 Research Section A: Accelerators, Spectrometers, Detectors and Associated Equipment 362 (2) (1995) 487 498. doi:
 https://doi.org/10.1016/0168-9002(95)00274-X.
 - URL http://www.sciencedirect.com/science/article/pii/016890029500274X